On the probabilistic representation of the wind climate for calibration of structural design standards

Michele Baravalle [a,*], *Jochen Köhler* [a]

[a] *Dept. of Structural Engineering, Norwegian University of Science & Technology, Rich. Birkelandsvei 1A, 7491 Trondheim, Norway*

ABSTRACT:

The article presents a contribution to the current debate on the probabilistic representation of the wind speed extremes for calibration of the partial safety factor covering wind action. The requirements for the probabilistic model are formulated. The Gumbel distribution is shown to represents best the 10-minutes mean wind velocity yearly maxima based on theoretical considerations and analyses of real data with different statistical techniques. Data from locations across a large geographical region indicate that the coefficient of variation of the distribution varies over the territory. A method is proposed for accounting this variation in order to calibrate a single partial safety factor for the whole territory. The distribution location is indirectly given in design standards through the georeferenced characteristic wind speed values. A solution for including the uncertainty affecting these values is suggested. The findings are implemented in an illustrative calibration exercise. The proposed methods and concepts might be applied to other environmental actions such as the snow loads.

KEYWORDS: wind actions, probabilistic modelling, code calibration, partial safety factors, extremes.

1 Introduction

Modern structural design codes or standards as the Eurocodes [1] provide simple and safe basis for the design of structures. The simplicity is achieved mainly by the fact that structural safety is checked by comparing the design values of action effects with the design value of the resistance. Semi-probabilistic design equations in the Load Resistance Factor Design format (LRFD, see e.g. [2]) use partial safety factors (PSFs) applied on the resistance and action sides. These factors control the reliability of the corresponding design solutions. Their values are selected by code committees in order to achieve the desired level of safety [2, 3, 4, 5]. In the present version of the European Standards (The Eurocodes [1]), for example, one single partial safety factor ($\gamma_Q = 1.50$) is recommended for all unfavourable environmental variable actions such as snow and wind. However, it has been shown in [6] that a wind load dominated structure designed with $\gamma_Q = 1.50$ has a reliability lower than the Eurocode target, which requires a yearly target reliability index β_t equal to 4.70 (for consequence class 2). It also appears reasonable to differentiate the partial safety factors of the environmental actions, such as snow, wind and temperature, since these actions originate from different physical phenomena and are represented by different models involving various random variables.

Modern calibration methods are based on reliability theory considering fully probabilistic models [3, 4, 7]. If wind action is involved, this requires models representing the wind action on structures from the basic physical

* Corresponding author at: Dept. of Structural Engineering, Norwegian University of Science & Technology, Rich. Birkelandsvei 1A, 7491 Trondheim, Norway.
E-mail address: michele.baravalle@ntnu.no

phenomenon (i.e. the geostrophic wind), and the representation of the governing variables, which may have a deterministic or a random nature. A widely accepted model is the Alan G. Davenport wind load chain [8] illustrated in Figure 1. Many semi-probabilistic codes such as the Eurocode 1 [9] represent wind actions on structures based on this model. The chain model includes five fundamental aspects, shortly: i) the *wind climate* comprising the weather systems generating geostrophic winds due to temperature gradients on the Earth surface; ii) the *influence of terrain*, which modifies the wind flow in the atmospheric boundary layer; iii) the *aerodynamic effects* depending on the structure shape; iv) the *dynamic effects* of the structure, and v) the *criteria* for verifying the predicted load models. More details are given in [10, 11].

Figure 1 – Alan G. Davenport wind loading chain.

Although the model is widely accepted, challenges are still faced when defining the probabilistic models representing different aspects. In fact, several probabilistic models for representing the aspects in the Davenport chain have been proposed for calibration of design codes, see e.g. [12]. Therefore, this article discusses some open issues related to the stochastic modelling of the 10-minutes mean wind velocity yearly maxima ($V_{b,\max}$) used for representing the *wind climate* for code-calibration purposes. In detail, the following aspects are addressed:

- *The selection of the type of distribution function representing* $V_{b,\max}$. This is still openly discussed in the scientific community since several distributions seem to fit well the available data, but they result in different calibrated safety factors due to the so-called tail sensitivity problem affecting the reliability analyses. Gumbel, Generalised extreme, Weibull, three-parameters Lognormal and other distributions are proposed in the literature, see for example [11, 13, 14].
- *The estimation of the distribution parameters that are relevant for the calibration of partial safety factors. These parameters are the coefficient of variation (*COV*) and the uncertainty on the distribution location*. The former should include the aleatory uncertainty (random nature of wind) and the epistemic uncertainties (originated by the lack of knowledge and a limited amount of information). The latter should include the uncertainties originated from the (surrogate) models utilized for creating the wind maps included in the design codes.
- *The representation and inclusion of the* $V_{b,max}$ *space-variation in the partial safety factor calibration*. This is required since a single partial safety factor for wind action is used for large geographical areas, although the wind climate is highly regional dependent.

The selection of the distribution type, the estimation of its parameters and their variation over a vast territory are addressed in Section 2 of the article. The second part of the article proposes a method for integrating, in the partial safety factor calibration, both the space-variation of the wind characteristics and the uncertainty on the distribution location. Wind speed records from five weather stations across Norway were analysed for catching the space-variation. The uncertainty on the distribution location was estimated based on measurements in several places over the territory. The findings are implemented in an illustrative calibration exercise.

2 Representation of the *wind climate*

2.1 Requirements of the model

The variation of the *wind climate* can be described by the wind velocity averaged over a period corresponding to frequencies in the spectral gap of the horizontal wind speed spectra [10, 15]. Periods of 10 minutes to 1 hour are typically used [16]. In the European Standard Eurocode 1 Part 1-4 (EC1-1-4) [9], the *wind climate* variation is represented by the basic wind velocity (V_b) which is defined as the 10-minutes mean wind velocity, irrespective of wind direction and time of the year, at 10 meters above the ground level in open terrain. The reliability

assessment of a structure exposed to wind actions is a time-variant problem since the wind is varying in time. The reliability problem can be simplified to a time-invariant problem, if it can be assumed that the resistance is independent of the wind process, by the so-called time-integrated approach (see [2]) considering the V_b yearly maxima $V_{b,\max}$.

As any random variable, $V_{b,\max}$ might be represented by a distribution function, which is in general defined by the *type* of distribution and its *parameters*. The parameters determine the *location*, *scale* and *shape* of the distribution, while the *type* determines the tail behaviour.

The *type* of distribution and the *coefficient of variation* COV (i.e. the scale or scatter independent of the location) play an important role in reliability-based code calibration. This role can be observed in Eq. (1) where the partial safety factor for a Gumbel distributed variable X is determined using the design value method [1]. In the Equation, β_t is the target reliability, α is the sensitivity factor (see, e.g., [2]), p_k is the fractile corresponding to the characteristic value, $\Phi(\cdot)$ is the standard normal cumulative density function and $a_{EM} \cong 0.5772$ is the Euler-Mascheroni constant. The analytical expressions of the distributions functions utilised in the article are given in Appendix A.

$$\gamma_X = \frac{6\,COV_X \ln\left\{-\ln\left[\Phi\left(\alpha\,\beta_t\right)\right]\right\} + 6\,a_{EM}\,COV_X - \pi\sqrt{6}}{6\,COV_X \ln\left\{-\ln\left[p_k\right]\right\} + 6a_{EM}\,COV_X - \pi\sqrt{6}} \tag{1}$$

The distributions *location* or magnitude is not affecting the partial safety factor when the extreme wind speeds are originated from a single physical phenomenon. In this case, standardised random variables can be used for PSF calibration as in [5]. For the wind, this is advantageous since the magnitude varies considerably in space due to different local climates and exposures. Design codes provide the regional magnitude or distribution location through the $V_{b,\max}$ characteristic value. In the Eurocode 1 [9], the characteristic value corresponds to the 98 % fractile (i.e. $p_k = 0.98$) of the yearly extreme value distribution and is referred to as the fundamental value of the basic wind velocity $v_{b,0}$. The regional distribution of $v_{b,0}$ is given in the Eurocode 1 National Annexes in the form of tables or maps. It has to be highlighted that the uncertainties affecting $v_{b,0}$ do influence the calibration of the partial safety factor. Thus, a good probabilistic representation of these uncertainties is of importance.

Correspondingly, in the authors' view, the distribution function representing $V_{b,\max}$ should have the following properties:

a) The distribution function type should represent $V_{b,\max}$ in the whole geographical application area of the standard under consideration.
b) The distribution function type and parameters have to be validated by recorded time series over an adequate period, say, longer than 15 years [17].
c) The distribution function type must agree with the phenomena generating randomness.
d) The stochastic model should be suited for the reliability methods used in the calibration procedure. Usually, a parametric probability distribution is sought since the first order reliability method (FORM) is commonly used in calibration of partial safety factors because of its accuracy and its low computational cost.
e) It should include the statistical uncertainties which arise from the lack of data and the model uncertainties in order to estimate the predictive reliability index, see e.g. [18].
f) It should be accurate in the upper tail defined as the surroundings of the design point. The fractile corresponding to the design point is approximatively equal to $\Phi(\alpha \cdot \beta_t) = 5 \cdot 10^{-4}$, which is the fractile associated with the design point of the wind induced action obtained with $\alpha = 0.7$ and $\beta_t = 4.7$ according to [1].

In principle, different types of distributions can be fitted to the data upper tail, and the best one can be individuated by using statistical tools, probabilistic reasoning and judgment. Nevertheless, the point c) above is of particular importance especially due to the lack of observations in the surrounding of the design point. The

application of extreme value theory (see e.g. [19, 20]) does limit the choice of distribution function type correspondingly, see also [21] for further discussion.

In the following, different analyses techniques are selected and utilised for individuating the distribution function representing the wind speed yearly maxima having all the properties listed above. These techniques differ in the basic assumptions, data considered and output. The techniques are divided into two main groups. The first group is based on the classical extreme value theory, which proposes different asymptotic distributions representing maxima under some specific assumptions that are discussed and assessed. The asymptotic convergence is improved when the parent distribution is considered. The distribution parameters are estimated from the yearly maxima, implying that one measurement for each year is considered only. The second group of techniques makes use of a larger amount of data by analysing the rate of threshold exceedance. These techniques allow to estimate the parameters as well as to evaluate the type of distribution that best represents the maxima.

The three-parameters lognormal (LN3) is proposed as a possible candidate distribution type for the representation of extreme wind phenomena [13]. The authors believe that, compared to other distributions discussed later, the distribution provides just a better fit to some samples of data due to the third parameter. In any case, the goodness of fit in the upper tail region of interest cannot be assessed due to lack of data. Nevertheless, the 3LN distribution was excluded because the distribution representing the N-years maxima ($V_{b,\max N}$) derived from LN3-distributed yearly maxima, as $F_{V_{b,max\,N}} = F_{V_{b,max}}^{N}$, is not of the type LN3. This is neither reasonable nor practicable since the type of distribution should not change with the selected reference period (for reference periods that are long enough to ensure independence between maxima). Therefore, this distribution is excluded in this paper since no theoretical background is found supporting its use.

2.2 Data set

Records from the Norwegian Meteorological Institute (MET) [22] of the highest hourly and 6-hours 10-minutes mean wind speed (MET code: *FX_1* and *FX*, respectively) were analysed. In detail, the 10-minutes mean wind speed was measured for each 10-minutes, and only the highest in each hour or in each 6-hours-period was recorded. *FX* records cover time periods between 25 and 58 years long. The data are of poor quality since the records are affected by rough rounding especially before 1980 (see Table 1). Nevertheless, no better data are available in Norway for periods long enough to support the probabilistic modelling of yearly maxima. Five stations across Norway were selected (see Figure 2) for representing different geographical regions. For illustration purposes, the data for Torsvåg Fyr (TOR) are reported in Table 1. *FX_1* records (Figure 3) are more accurate since rounded at $\pm 0.05\,m/s\,(=0.1kn)$ but they are available for periods not longer than 22 years. In general, a good agreement between *FX* and *FX_1* was observed in periods covered by both datasets. The data were quality checked, and two corrections were done for TOR data that included two entries equal to $45.2\,m/s$. These measurements were considered erroneous because of the extreme magnitude and due to the absence of reports on major storms in the corresponding period. Linear interpolation between previous and posterior entries was used for correcting the corresponding records.

Figure 2 – Weather stations (from Google My Maps).

Table 1 – FX values for TOR in m/s *converted from knots (kn) (rounding:** $\pm 2.31 m/s (= 4.5 kn)$ *, §* $\pm 1.80 m/s (= 3.5 kn)$ *,* $\pm 0.26 m/s (= 0.5 kn)$ *otherwise).*

Year	v_b	*Year*	v_b	*Year*	v_b	*Year*	v_b
1957	*26.75**	*1969*	*22.64§*	*1981*	*30.87§*	*1993*	*36.01*
1958	*30.87§*	*1970*	*26.75**	*1982*	*27.78*	*1994*	*22.64*
1959	*34.98**	*1971*	*26.75**	*1983*	*25.72*	*1995*	*26.75*
1960	*22.64§*	*1972*	*26.75**	*1984*	*27.78*	*1996*	*34.98*
1961	*22.64§*	*1973*	*26.75**	*1985*	*26.75*	*1997*	*34.98*
1962	*22.64§*	*1974*	*30.87§*	*1986*	*24.18*	*1998*	*27.78*
1963	*26.75**	*1975*	*26.75**	*1987*	*26.75*	*1999*	*22.12*
1964	*22.64§*	*1976*	*26.75**	*1988*	*25.72*	*2000*	*29.32*
1965	*26.75**	*1977*	*26.75**	*1989*	*33.95*	*2001*	*26.24*
1966	*22.64§*	*1978*	*26.75**	*1990*	*34.98*	*2002*	*24.18*
1967	*22.64§*	*1979*	*22.64§*	*1991*	*39.10*	*2003*	*26.75*
1968	*30.87§*	*1980*	*26.75**	*1992*	*25.21*	*2004*	*23.15*

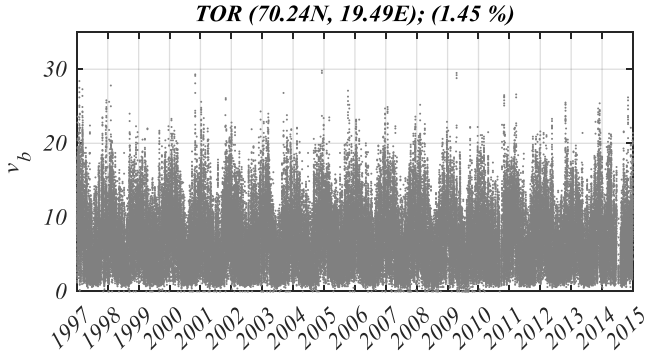

Figure 3 - FX_1 series for TOR station with station coordinates and percentage of missing measurements (units: m/s *).*

2.3 Assumptions and limitations

The data were analysed under the following assumptions, limitations and simplifications.

a) Data from one location were considered sampled from the same population although the physical phenomena producing extreme wind velocity realisations might be different (e.g. extra-tropical cyclones, thunderstorms, etc.). This simplification was set to be consistent with the level of detail of the current version of the Eurocode 1, which includes a unique model for wind loads based on extra-tropical cyclone generated winds.

b) The *wind climate* was considered independent from the *influence of terrain* since the latter creates turbulences characterised by temporal frequencies that differ from the wind climate frequencies by

one or two orders of magnitude, see e.g. [11]. This approximation is also considered in the Eurocode 1 [9].

c) Despite the fact that wind direction is important when the structural resistance and the wind are direction-dependent, see e.g. [23], wind directionality was not considered in the analyses. The reasons are that i) considering structures with direction-independent resistance only (or equivalently considering the wind worst direction) is conservative; ii) directionality is highly location-dependent reducing the generality of the model which is sought; iii) the basic wind velocity in the Eurocode 1 is not conditional on a specific wind direction that is accounted by the direction factor.

d) The number of missing measurements is low for all the stations (see Figure 3) and it was assumed that the lack of registration was not correlated to extreme wind speeds.

e) The five selected measurement locations are located in small islands close to the shore or on the coast. The locations are surrounded by open terrain and by open sea. The latter has a lower roughness compared to open country. Nevertheless, when extreme wind speeds are registered, the sea is assumed in "ultimate limit state" and, hence, presenting the same roughness as the open country (see [16] Annex C). Therefore, the surroundings of the measuring stations are assumed to have a terrain roughness equivalent to the category II of the Eurocode 1, which is the reference category for deriving the basic wind velocity (V_b) according to [9].

f) The effects of the climate change on the wind speed are not considered, i.e. the wind is assumed to be an ergodic process. Although the climate change is predicted to affect the wind speed in future (see e.g. [24]), its inclusion in the design standards should involve several disciplines [25] and was not part of the current study.

2.4 Classical extreme value theory

According to the classical extreme value theory, the maxima of independent, identically distributed variables tend to a Gumbel distribution (see Eq. (A.1)) under the following assumptions [19]: *i*) the number of independent realisations is constant, and *ii*) the parent distribution has an exponential tail. These assumptions do not seem to be strictly verified for the 10-minutes mean wind speed since the number of independent weather systems and the parent distribution representing the 10-minutes mean wind speed differ from year to year. However, for practical analyses, the annual maxima present a linear behaviour in the Gumbel plot meaning that the assumptions are not strongly violated [17] and suggesting the Gumbel as the asymptotic distribution. The most accurate method for fitting the Gumbel distribution to the data is the so-called Gumbel-Lieblein method as shown in [26]. Nevertheless, the distribution parameters were estimated in this work utilizing the maximum likelihood (ML) method since it allows accounting for the rough rounding characterising the data under consideration. The likelihood is formulated as a function of the distribution parameters conditional to the observations and the selected distribution function. The validity of the assumed distribution can be assessed based on the magnitude of the maximum (also relative to the maxima that correspond to different assumed distribution types). The deviation of the (unknown) real distribution is partly reflected (and considered) by the covariance of the parameters. In addition, the ML method provides the estimates of the parameters uncertainty which is integrated into the predictive distribution $f_X(x)$ in Eq. (2),

$$f_X(x) = \int_{\boldsymbol{\Theta}} f_{X|\boldsymbol{\Theta}}(x \mid \boldsymbol{\theta})\, f_{\boldsymbol{\Theta}}(\boldsymbol{\theta})\, d\boldsymbol{\theta} \tag{2}$$

where: $\boldsymbol{\Theta}$ is a vector with the distribution parameters and $f_{\boldsymbol{\Theta}}(\boldsymbol{\theta})$ is the joint density function representing the parameter uncertainties. These uncertainties might be significant when the data are limited in number or have poor quality. The ML method also allows considering the rounding and the left censoring by using the likelihood function reported in Eq. (A.2). The use of left censored data allows to fit better the upper tail but it requires an adequate number of years of records for having a sufficient number of observations in the tail. The selection of the

censoring threshold is not trivial. In fact, high thresholds lead to significant variance in the estimates while low thresholds produce estimations biased toward the central part of the distribution.

The distributions fitted to the measurements in TOR are illustrated in Figure 4. Data censoring improved the upper tail fit, and simultaneously increased the statistical uncertainty leading to a fatter tail of the predictive distribution. The predictive distributions were obtained with Eq. (2). The integral was approximated numerically by Monte Carlo (MC) sampling. Consequently, the predictive could not be represented in a closed form. Therefore, its upper tail was approximated by a Gumbel distribution obtained fitting the highest 30 % of the sampled values (i.e. the values characterised by $-\ln\left(-\ln\left(F_{V_{b,\max}}\right)\right) > 1.0$ in Figure 4) since these data were observed lying on a straight line in the Gumbel probability plot. The estimated *COVs* of the Gumbel distribution are displayed in Figure 5 as a function of the censoring threshold v_c. Their order of magnitude agrees with the values given in [27]. *FX* data were used only when the more precise *FX_1* data were missing. The largest censoring thresholds were approximatively corresponding to the 70 % fractile values.

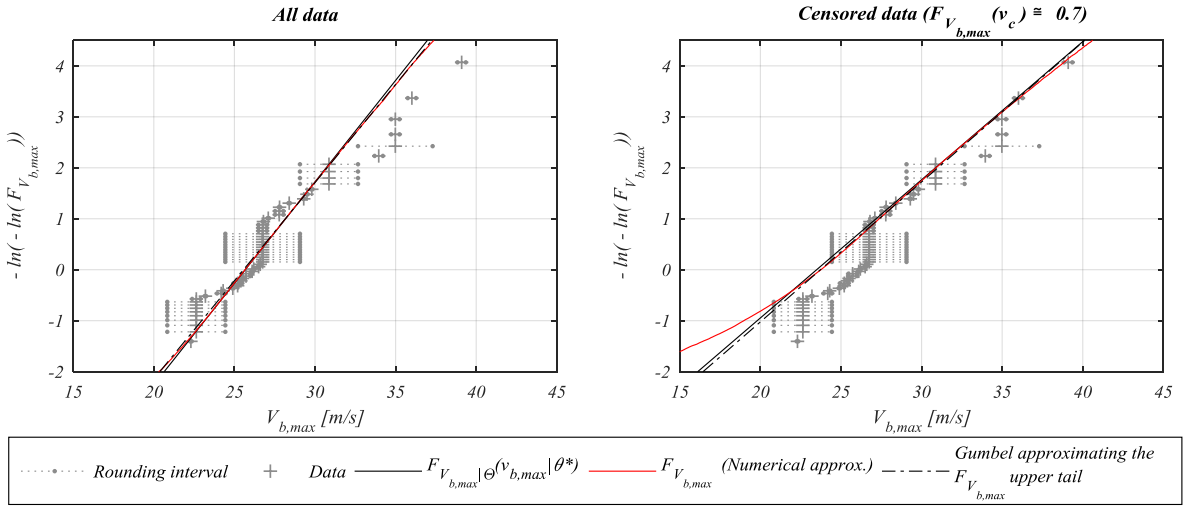

Figure 4 – Gumbel probability plot with measured data (FX and FX_1) for weather station TOR and fitted Gumbel distributions. Data sorted according to the central values of the rounding intervals. Predictive distributions approximated by Montecarlo sampling with 10^5 simulations.

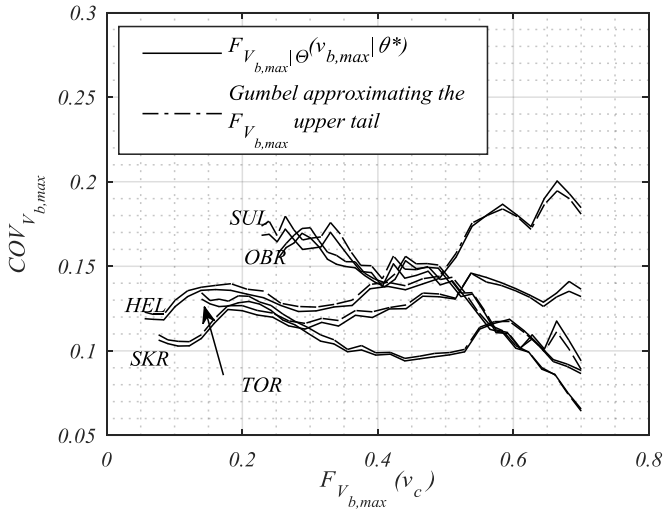

Figure 5 – $COV_{V_{b,max}}$ for Gumbel distributions estimated varying left-censoring threshold v_c on FX and FX_1.

2.4.1 Classical extreme value theory considering parent distribution

A significant amount of information contained in the weather data is not utilized when yearly maxima are analysed. Additional information can be included considering the underlying statistic. The probability distribution representing the 10-minutes mean wind speeds (i.e. the basic wind velocity V_b) is referred to as the "parent

distribution" in the following. The parent distribution is the distribution from where the extreme wind speeds are "sampled". In Europe, the distribution that best represents V_b is the Weibull (see Eq. (A.4)) with shape parameter $b_w(V_b) \in [1.8, 2.2]$ as extensively reported in the literature and supported theoretically by the study of Harris and Cook [28]. It follows that the so-called preconditioned random variable $V_b^{b_w}$ is exponentially distributed (i.e. Weibull distributed with unitary shape parameter). The maxima of the exponentially distributed random variable $V_b^{b_w}$ converge faster than V_b to the Gumbel distribution. Consequently, the "*penultimate*" extreme value distribution for $V_b^{b_w}$ corresponds to the "*ultimate one*" [29] meaning that the error when using Gumbel asymptote is reduced. Cook introduced first this procedure considering a preconditioning parameter equal to 2 [24]. The obtained variable, V_b^2, is proportional to the 10-minutes mean wind pressure ($1/2\,\rho V_b^2$) and is represented by a Weibull distribution with $b_w(V_b^2) = b_w(V_b)/2$. $b_w(V_b^2)$ is close to one for $b_w(V_b) \in [1.8, 2.2]$ and, hence, V_b^2 is close to exponentially distributed.

The Gumbel distribution *COVs* estimated from the preconditioned data were around double than for non-preconditioned data, see Figure 6. In addition, it was observed that the *COV* variation for different censoring thresholds and the variation among different weather stations were of the same order of magnitude. This made the selection of the censoring threshold less critical as a generalised representation of the *COV* was sought. The change of trends in Figure 5 and Figure 6 shows that the characteristics of the upper tail are caught by censoring fractiles above, approximatively, 50 %. For the data analysed, a censoring threshold corresponding to fractiles around 60 to 70 % was judged to balance the statistical uncertainty on the parameter estimates and the accuracy in the upper tail. The chosen censoring fractiles have no general validity since they depend on the data set under consideration and on the part of the distribution that is of interest (see Section 2.1), therefore they are case specific. In general, higher censoring thresholds might be selected when longer time series are available and data have better quality.

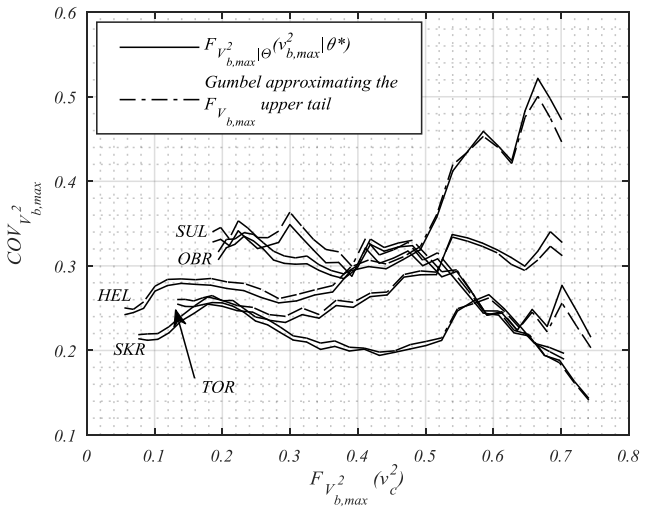

Figure 6 – $COV_{V^2_{b,max}}$ for Gumbel distributions estimated varying left-censoring threshold v_c on FX and FX_1. Predictive distributions approximated by Montecarlo sampling with 10^5 simulations.

The knowledge on the parent distribution allows estimating the error affecting the use of asymptotic distributions. Assuming that the Weibull parent distribution F_X is known, the (theoretically) exact distribution of maxima is obtained from Eq. (3), where r is the number of independent events per years.

$$F_{X_{max}}(x) = \left[F_X(x \mid a_w, b_w)\right]^r \tag{3}$$

This derivation is not directly used since small errors on r, b_w, a_w lead to significant errors in $F_{X_{max}}$. Nevertheless, Eq. (3) can be utilised for estimating the errors induced by approximating the exact $F_{X_{max}}$ with a Gumbel distribution. The error affecting the design point resulting from this approximation is depicted Figure 7 (reproduced after [29]). The error is in the order of $\pm 2\%$ for a Weibull distributed variable with $b_w \approx 1$ like V_b^2, and much

larger for a variable with $b_w \approx 2$ like V_b. Therefore, it can be concluded that the use of the preconditioned wind speed is advantageous for calibration of codified design since the convergence error on the part of the upper tail of interest is almost eliminated. The values of $COV_{V_{b,max}^2}$ obtained from Eq. (3) are depicted in Figure 8 and are compared with the Gumbel asymptote obtained with asymptotic parameters given in [30]. They agree quite well with the values obtained in the data analysis, see Figure 5. This verifies the hierarchical model which considers Weibull parent and Gumbel maxima. More importantly, the results obtained from this hierarchical model (Figure 8) suggest that the $COV_{V_{b,max}^2}$ values over the territory of interest are not expected to differ much from the ones obtained analysing the five selected locations since the same weather system is originating the wind over the territory under consideration. Therefore, the use of few representative locations is sufficient for individuating a generic representation of the wind climate.

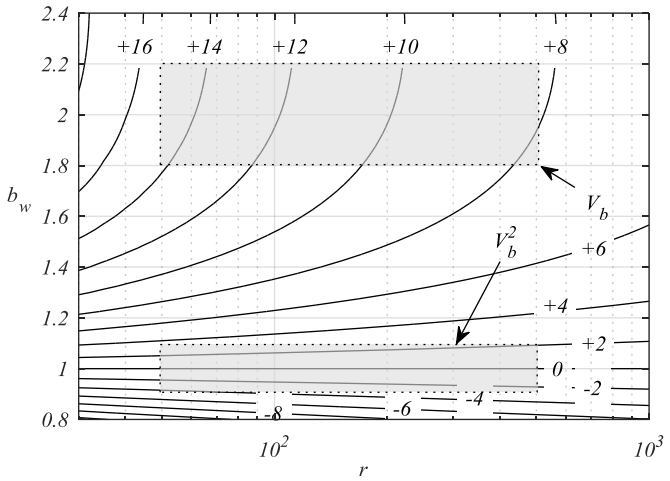

Figure 7 – Error in percentage affecting the design value $\left[\tilde{F}_{X_{max}}^{-1}\left(\Phi\left(\alpha\cdot\beta_t\right)\right)-F_{X_{max}}^{-1}\left(\Phi\left(\alpha\cdot\beta_t\right)\right)\right]\Big/F_{X_{max}}^{-1}\left(\Phi\left(\alpha\cdot\beta_t\right)\right)$ *for* $\alpha=0.7$, $\beta_t=4.7$ *and* $\tilde{F}_{X_{max}}$ *being the Gumbel distribution approximating the exact distribution of maxima* $F_{X_{max}}$. *Grey areas represent possible domains of* r *and* b_w *for wind speed.*

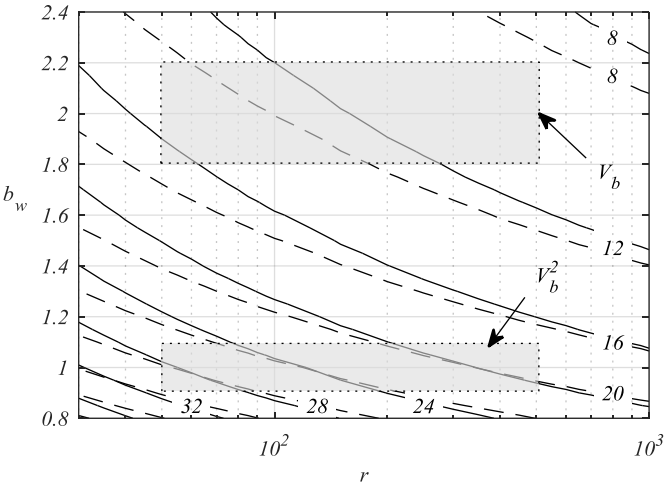

Figure 8 – Yearly maxima distribution COV from exact formula Eq. (3) (dashed line) and Gumbel asymptotic approximation (continuous line). Grey areas represent possible domains of r *and* b_w *for wind speed.*

2.4.2 Generalised extreme value distribution

A more general application for the analysis of extreme wind velocity data makes use of the Generalised Extreme Value distribution which includes three types of distributions (Gumbel, Fréchet and Weibull maxima) characterised by three different tail behaviours. The data indicates which type of distribution is better through inference on the shape parameter (ξ_{GEV}) (see e.g. [20]). The uncertainty on the estimated parameter ($\hat{\xi}_{GEV}$) can be interpreted as the uncertainty on the distribution and tail type. It has to be noted that, when the statistical

uncertainty is neglected, the GEV distribution always fits better the data compared with the Gumbel distribution due to the third additional parameter. Nevertheless, due to the asymptotic property of GEV, convergence errors still affect the estimate, see e.g. [29]. As reported in the literature, $\xi_{GEV} < 0$ is typical for 10-minutes mean wind speed yearly maxima, implying that the distribution tail converges to a limit value being the domain right-bounded $\left(-\infty; a - b/\xi_{GEV}\right]$.

The GEV shape parameters estimated from the data were affected by high uncertainty. A standard deviation in the order of 0.3 was obtained. In addition, some most likely values of the shape parameters were positive (see Table 2) corresponding to distributions defined on a lower bounded domain. Unreasonable and very unstable COV and $\hat{\xi}_{GEV}$ were estimated from censored data with different censoring threshold. All these results were believed to be a consequence of the fact that the limited number of data points and their low quality led to considerably high statistical uncertainty on the parameter estimates. In fact, it is shown in the literature that a limited amount of data leads to unreasonable GEV parameters [31]. This deficiency is related to the ML estimation. In case the GEV distribution was to be used, the Bayesian estimation could have provided better parameter estimates combining the available measurements with the experts' belief by selecting appropriate priors. However, this technique was not applied since the GEV distribution was excluded based on the analyses presented in the remaining part of the article.

The results obtained from non-censored data need careful interpretation. The authors believe that GEV provides only a better empirical fit to the data for two reasons. The first is that the GEV distribution always provided greater Akaike Information Criteria (AIC) scores compared to the Gumbel and, thus, Gumbel is to be preferred [32]. The largest differences in AIC scores were observed for censored data. In detail, $AIC = 2k - 2\ln\left(\hat{L}\left(x \mid \hat{\boldsymbol{\theta}}, M\right)\right)$, where M is the selected statistical model with k parameters (e.g., Gumbel with $k = 2$, and GEV with $k = 3$), and $\hat{L}\left(x \mid \hat{\boldsymbol{\theta}}, M\right)$ is the maximum likelihood of the data x (corresponding to the parameters $\hat{\boldsymbol{\theta}}$ estimated with the ML). The second reason is that, as also commented in [29], the domain limits for GEV distributions representing $V_{b,max}^2$ and $V_{b,max}$ were inconsistent, and did not correspond to the natural domain limits of the variables, see Table 2. For example, for OBR location, the parameters estimated from $V_{b,max}$ gave a domain upper bound equal to $44.1 m/s$, while the estimates from $V_{b,\max}^2$ gave an upper bound of $2746\left(m/s\right)^2 = (52.4 m/s)^2$. Further, in [29] it was proven that Weibull parents with $b_w = 2$ and 1 give $\xi_{GEV} \cong -0.1$ and 0, respectively. The fact that the average values of $\hat{\xi}_{GEV}$ in Table 2 are very close to these values and that all the $\hat{\xi}_{GEV}$ 90 % confidence bounds contain -0.1 can be seen as an indirect proof that the assumption of a Weibull distributed parent and therefore asymptotically Gumbel distributed maxima leads to a good representation of data. Based on the observations above, the use of GEV distribution is excluded.

Table 2 – Estimated GEV shape parameter and coefficient of variation from FX and FX_1.

	***GEV* – $V_{b,max}$**			***GEV* – $V_{b,\max}^2$**		
	$\hat{\xi}_{GEV}$	***COV* (conditional)**	***Domain***	$\hat{\xi}_{GEV}$	***COV* (conditional)**	***Domain***
HEL	*-0.313*	*0.14*	$(-\infty; 37.3]$	*-0.256*	*0.26*	$(-\infty; +1391]$
OBR	*-0.191*	*0.13*	$(-\infty; +44.1]$	*-0.087*	*0.26*	$(-\infty; +2746]$
SKR	*0.068*	*0.11*	$[-6.1; +\infty)$	*0.161*	*0.25*	$[-33.1; +\infty)$
TOR	*0.135*	*0.14*	$[+22.4; +\infty)$	*0.234*	*0.32*	$[+134.2; +\infty)$
SUL	*-0.326*	*0.14*	$(-\infty; +41.5]$	*-0.209*	*0.28*	$(-\infty; +1942]$

2.5 Threshold exceedance analysis

The analysis of yearly maxima excludes a significant amount of available data in contrast with methods based on analysing exceedances, exceedance rates and peaks over threshold as illustrated in Figure 9. Certain results are reported in this Section for the weather station TOR only, similar trends and behaviours were observed for the other four stations.

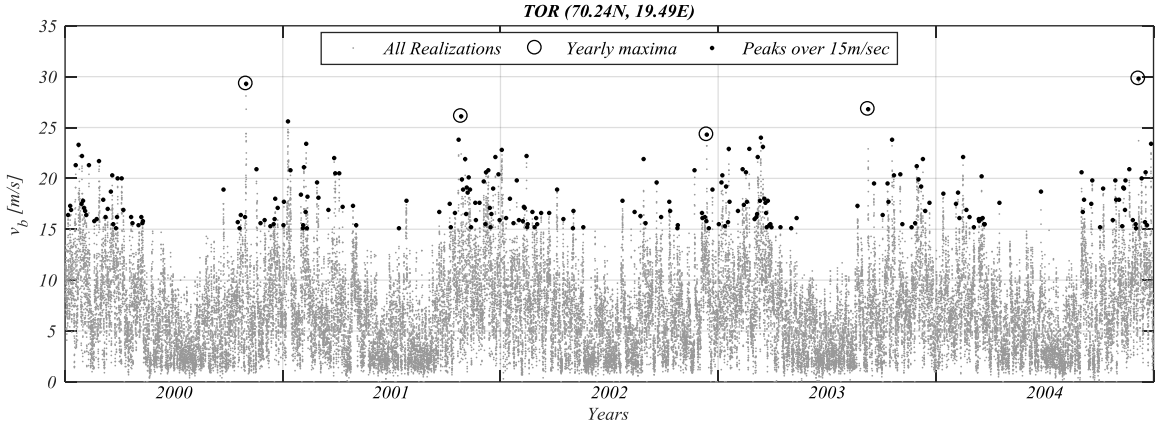

Figure 9 – FX_1 time-series between 01-01-2000 and 31-12-2004 with all recorded values, yearly maxima and independent peaks over the threshold $v_t = 15 m/\sec$.

2.5.1 The mean upcrossing rate

The mean upcrossing rate $\bar{\eta}^+(v_t)$ functional relationship with the threshold v_t provides significant information about the distribution of maxima. The starting point is Eq. (4) which relates $F_{V_{b,max}}$ to $\bar{\eta}^+(v_t)$, where T is the reference period equal to one year.

$$F_{V_{b,max}}(v_t) = \exp\left\{-\bar{\eta}^+(v_t)\cdot T\right\} \tag{4}$$

The up-crossing rate for large enough thresholds $v_t > v_{t,0}$ is usually related to v_t through a function of the form $\bar{\eta}^+(v_t) = \tilde{q}(v_t)\exp\left\{-a(v_t - b)^c\right\}$; where a, b, c are constants and $\tilde{q}(v_t)$ is near-constant [33]. The case $c = 1$ gives $\ln\left(\bar{\eta}^+(v_t)\right)$ linear in v_t and corresponds to Gumbel asymptote. On the contrary, cases with $c \neq 1$ represent sub-asymptotic behaviours.

Up-crossings of a threshold are in general dependent. De-clustering is performed for extracting independent events considering clusters to start (and end) when at least n_c consecutive values are below a threshold v_t, see e.g. Coles [20]. The average number of up-crossings (or cluster) over a defined period (e.g., one year) is referred to as the average conditional exceedance rate (ACER) $\varepsilon_{n_c}(v_t)$. The empirical ACER functions are estimated from the data by the ACER method and can be used instead of $\bar{\eta}^+(v_t)$ in the above equations [34].

The plots of $\ln\left(\varepsilon_{n_c}(v_t)\right)$ versus v_t for the analysed data show the dependencies between up-crossings. It was observed that $n_c > 4$ eliminates the dependency without affecting the upper tail, see Figure 10. Thus, upcrossings separated by 4 or more hours are considered independent or, equivalently, belonging to different storm events. On the contrary, upcrossings separated by less than 4 hours might belong to the same storm and thus be dependent. This is in accordance with the average duration of a storm that is indicated in [27] to be in average 8 hours. For $n_c = 4$ the fitted line had $c \neq 1$ for V_b meaning sub-asymptotic behaviour and $c \cong 1$ for V_b^2. This further proves that the wind speed maxima are sub-asymptotic while the preconditioned wind speed converges to the asymptote in the tail.

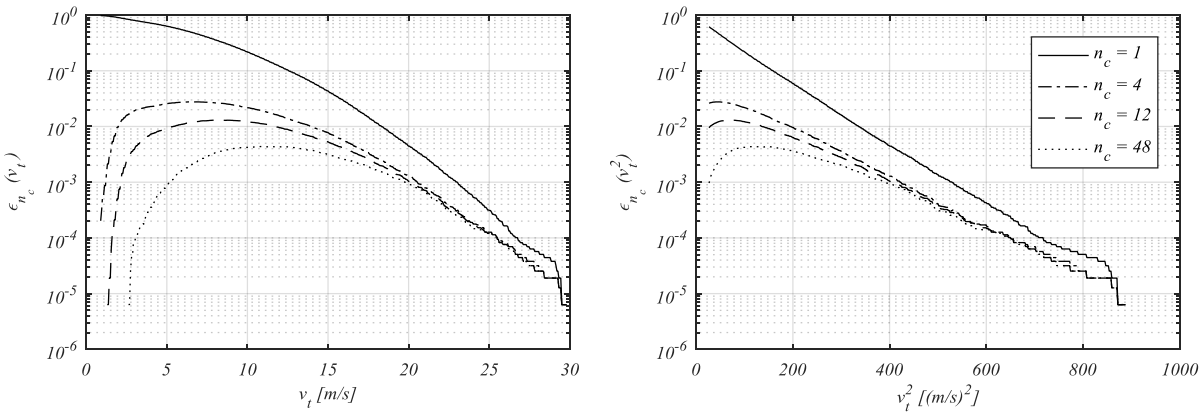

Figure 10 - Logarithm of the ACER versus threshold for wind speed (right) and wind speed squared (left) at TOR weather station obtained with the Matlab-based free software [35]. Estimated parameters with $n_c = 4$ for v_t : $a = 0.20$, $b = 13.58$, $c = 1.27$, $q = 0.01$; and for v_t^2 : $a = 0.01$, $b = 64.59$, $c = 1.00$, $q = 0.04$.

2.5.2 Peaks over threshold

Threshold exceedance analysis can also be utilised for evaluating the use of the GEV distribution and for estimating its parameters. In detail, the GEV shape parameter ξ_{GEV} is estimated by the Pickands method [36] analysing the peaks over threshold (POT). For large enough thresholds $v_t > v_{t,0}$ and under the assumptions that the realisations are independent, identically distributed and their maxima have a GEV domain of attraction, the distribution function of the exceedance $Y = V_b - v_t$ conditional on $V_b > v_t$ is represented by a generalised Pareto distribution (GPD). Pickands [36] proved that the GPD and the GEV distribution have the same shape parameter $\xi_{GEV} \equiv \xi_{GPD}$ asymptotically. Maximum likelihood estimates of $\hat{\xi}_{GPD}$ are reported in plots A in Figure 11. Data dependencies were eliminated by declustering data as described before. In this case, the largest value in each cluster was kept while the rest were discarded.

The POT analysis presents the non-trivial task of selecting the right threshold v_t. Different methods for threshold selection are proposed in the literature, see e.g. [37]. As discussed in [20], the following is valid for thresholds $v_t > v_{t,0}$: *i*) the mean of the exceedances $\bar{y}$ is linear in v_t ; *ii*) $\hat{\xi}_{GPD}$ is near-constant and the Pareto scale parameter $\bar{\sigma}$ is linear in v_t ; *iii*) the reparametrized GPD scale parameter $\sigma^* = \bar{\sigma}_{v_t} - \hat{\xi}_{GPD} v_t$ is constant. These three points can be used inversely for finding the appropriate $v_{t,0}$. For the TOR data, a minimum threshold $v_{t,0}$ of approximatively $15\,\mathrm{m/sec}$ was judged to satisfy all these three requirements as illustrated in plots B, C and D in Figure 11. Thresholds v_t larger than, but close to, $v_{t,0}$ should be selected for balancing statistical uncertainty and precision in the upper tail. Trends exactly equal to the theoretical ones cannot be expected due to inherent variability and the limited amount of data. The assessment of the appropriate threshold must be performed for each case and may be highly subjective and arduous in real problems.

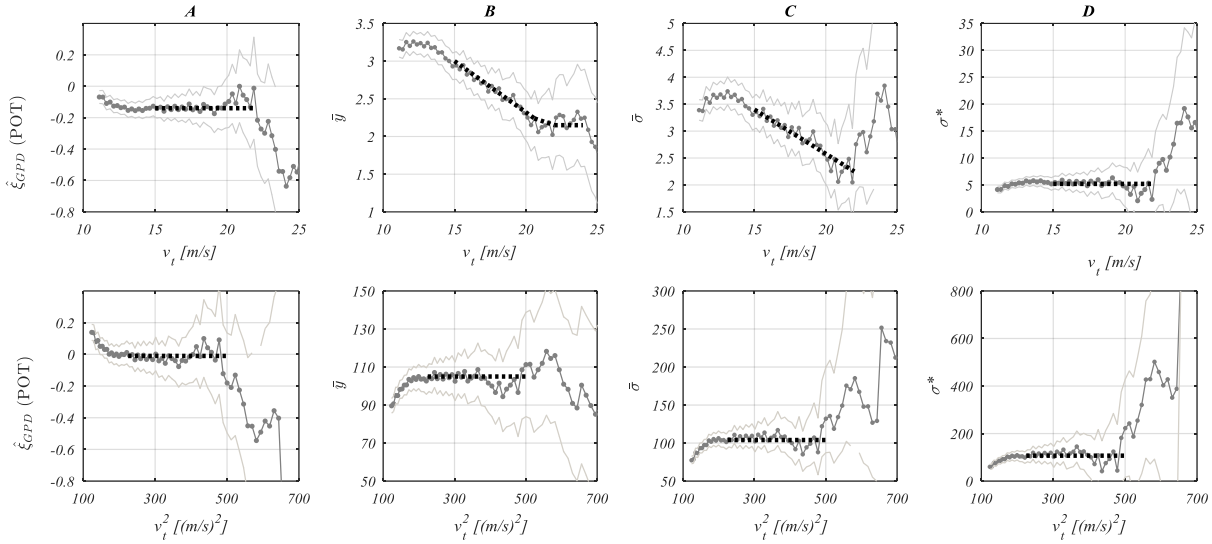

Figure 11 – ML estimates of $\hat{\xi}_{GPD}$ from POT method (A) and plots for selecting threshold $v_{t,0}$ (B, C and D) for wind speed (top) and wind speed squared (bottom) for weather station TOR. 90 % confidence intervals drawn with light grey lines for illustrating the statistical uncertainty; dotted lines were drawn manually for representing identified trends.

The plots in Figure 11 present trends that further support the selection of the Gumbel for representing the extremes of a Weibull parent. In details, the signs of $\partial\bar{y}/\partial v_t$ are equal to $\hat{\xi}_{GPD}$ as expected when the parent is Weibull as demonstrated in [38]; $\partial\bar{y}/\partial v_t$ for V_b decreases to zero with increasing v_t, and it is (near-)constant for V_b^2. This is in accordance with the relations derived in [29] based on the assumption of Weibull parent, and the $\hat{\xi}_{GPD}$ is negative for V_b (around - 0.1) and close to zero for V_b^2 reflecting the behaviour shown in [29]. In conclusion, all results from exceedance analyses were consistent with the assumption of Weibull parent and indicated Gumbel for representing maxima, as concluded from the analysis of yearly extremes.

An alternative approach for identifying the distribution *type* uses the tail heaviness index that is proportional to the negative of the curvature of the minus log-exceedance plot [30, 39]. In the authors' view, the method is a useful decision-making tool for selecting the distribution representing maxima when lacking information on the underlying phenomenon and theoretical background supporting one or another distribution type. Consequently, application of this method was not documented in this article since the knowledge on the underlying phenomenon originating wind extremes allowed proofing theoretically that the Gumbel distribution is best for representing maxima.

3 Inclusion of wind climate spatial variation in code calibration

The first part of the article shows that the partial safety factor depends on the COV (see Eq. (1)) and that the COV varies in space. At the same time, semi-probabilistic codes typically include only one partial safety factor for the wind actions over the entire territory. Therefore, this Section proposes a framework for calibrating the wind partial safety factor and suggests a method for accounting the space-variation of the climatic actions.

3.1 Representation of the wind action on structures

Reliability-based calibration of the wind partial safety factor uses reliability analyses where the wind action is represented probabilistically. The models given in [27], that have been used in other calibration works [14], were adopted in this work. The model is based on the Alan G. Davenport wind load chain illustrated in Figure 1. The wind action on structure yearly maxima (W_{max}) is modelled as $W_{max} = 1/2\,\rho C_d\, C_r\, C_a\, C_g\, V^2_{b,max}$. The air density ($\rho$) is considered deterministic since its scatter is small at large wind speeds [40]. The *influence of the terrain* is accounted by the roughness factor C_r and by the gust factor C_g. The former describes the variation of the mean velocity pressure with height, the latter is the ratio between the peak velocity pressure to the mean velocity pressure. The *aerodynamic effect* is accounted for by the shape factor C_a that is named external pressure coefficient C_{pe} when W_{max} is the external pressure. Similarly, the internal pressure and friction are obtained with the corresponding factors C_{pi} and C_{fr}. The structural *dynamic effect* is accounted for by the dynamic factor C_d. The C-factors are affected by aleatory and epistemic uncertainties, the details on the stochastic models representing them can be found in [27].

3.2 Reliability based calibration of partial safety factors

Following the methodology proposed by the JCSS [5], the partial safety factor (PSF) calibration is performed using a normalised and generalised limit state function as the one given in Eq. (5). The event of structural failure is characterised by $l(\mathbf{x}) < 0$.

$$l\left(x_R, r, g, c_d, c_{pe}, c_g, c_r, v^2_{b,max}\right) = z\, x_R\, r - \left[\delta g + (1-\delta)\, x_Q c_d c_{pe}\, c_g\, c_r\, v^2_{b,max}\right] \tag{5}$$

In the limit state function, δ is a parameter representing different proportions between permanent action g and wind action w, r is the material property dominating the failure mode, x_R is the resistance model uncertainty, x_Q the wind-load model uncertainty and z is the design variable governing the failure mode. This limit state function is generalised, i.e. it represents, with a satisfactory level of detail, different failure modes. For example, failure of a timber beam in bending is represented by r being the timber bending strength and x_R the model uncertainty on the bending capacity of timber elements. In addition, the limit state function is normalized, i.e. the random variables R, G and $V^2_{b,\max}$ have unitary mean. This allows for the simultaneous consideration of materials with different grades, and different load intensities. The normalisation and scaling of random variables, as for example by the factor $1/2\,\rho$, are 'absorbed' by z and simplify the problem without affecting the calibration outcome as discussed in the introduction.

The generic structural element is designed with a semi-probabilistic approach. An example of a design equation corresponding to the limit state equation in Eq. (5) is given in Eq. (6), where the Eurocode 0 [1] safety

format is used. $\gamma_M, \gamma_G, \gamma_Q$ are the material, permanent action and variable action partial safety factors, respectively. The subscript "k" indicates the characteristic value of the random variable.

$$z = z\left(\gamma_M, \gamma_G, \gamma_Q\right) = \frac{\gamma_M}{r_k}\left[\, \delta g_k\, \gamma_G + \left(1-\delta\right)\gamma_Q\, c_{d,k} c_{pe,k}\, c_{g,k} c_{r,k} v_{b,0}^2 \,\right] \tag{6}$$

In EC1-1-4, for example, the fundamental value of the basic wind velocity $v_{b,0}$ or velocity squared $v_{b,0}^2$ is defined as the 98 % fractile of $V_{b,\max}$ or $V_{b,\max}^2$, respectively. $v_{b,0}^2$ is calculated in Eq. (7) for the normalised $V_{b,\max}^2$ (i.e. $\mu_{V_{b,max}^2} = 1.00$) and a given geographical location (i.e. known $COV_{V_{b,\max}^2}$). The statistical uncertainty is integrated into the distribution and therefore included in the coefficient of variation hereinafter.

$$v_{b,0}^2 = v_{b,0}^2\left(COV_{V_{b,max}^2}\right) = -\frac{\left(6\, a_{EM} COV_{V_{b,max}^2} + 6\ln\left(-\ln\left(0.98\right)\right) COV_{V_{b,max}^2} - \pi\sqrt{6}\right)}{\sqrt{6}\pi} \tag{7}$$

The reliability index β associated with the limit state function in Eq. (5) is a function of the partial safety factors through the design parameter z, i.e. $\beta = \beta\left(z\left(\boldsymbol{\gamma}\right)\right)$. The calibrated safety factors are obtained imposing $\beta\left(z\left(\boldsymbol{\gamma}\right)\right) \equiv \beta_t$, where β_t is the target reliability index. When several design situations are considered simultaneously, calibration is performed by minimising the penalty function subject to the partial safety factors. Further details on calibration of design standards can be found in [2, 3, 5, 7, 41].

3.3 Wind action space-variation

Code calibration is generally performed for large interregional areas that correspond to the validity domain of the code format to be calibrated. In this area, the $COV_{V_{b,\max}^2}$ is varying as shown in Section 2 and this has to be taken into account in the calibration process. A possible strategy for providing a unique safety factor could be to choose conservatively a large $COV_{V_{b,\max}^2}$ which results in a large γ_Q. The selection of the largest value over the entire domain covered by the code under consideration includes some obvious difficulties. Alternatively, the variation of the $COV_{V_{b,\max}^2}$ in space is accounted by treating the $COV_{V_{b,\max}^2}$ explicitly as a random variable in the limit state function. The variation of the $COV_{V_{b,\max}^2}$ can include not only the variation over the space but also the statistical uncertainty and the uncertainty related to the selection of the appropriate censoring threshold. The new limit state function is given in Eq. (8) was obtained by including Eq. (7) in Eq. (6) and by expressing the random variable $V_{b,\max}^2$ in Eq. (5) as a function of a normal standard variable U and the distribution parameters a and b.

$$l\left(x_R, r, g, c_d, c_{pe}, c_g, c_r, x_a, u\right) = z\, x_R\, r - \left[\, \delta g + \left(1-\delta\right) x_Q c_d c_{pe}\, c_g\, c_r \left[\, x_a a - b\ln\left(-\ln\left(\Phi\left(u\right)\right)\right)\right]\right] \tag{8}$$

The parameters a and b for the normalised $V_{b,\max}^2$ are a function of the random variable $COV_{V_{b,\max}^2}$: $b = COV_{V_{b,max}^2}\sqrt{6}/\pi$ and $a = 1 - a_{EM} COV_{V_{b,max}^2}\sqrt{6}/\pi$. It is highlighted that the $COV_{V_{b,\max}^2}$ enters the limit state function through both the design parameter and the wind action term. The $v_{b,0}$ (or $v_{b,0}^2$) value for a specific location is, indeed, obtained from Eq. (7) with the $COV_{V_{b,\max}^2}$ characterising the maxima in that location.

The random variable X_a in Eq. (8) represents the uncertainty on the location of the distribution function $F_{V_{b,\max}^2}$ or, equivalently, the uncertainty on the fundamental value of the basic wind velocity squared $v_{b,0}^2$ provided in wind maps and tables. Therefore, X_a depends on the model used by the code committees for deriving the $v_{b,0}$ or $v_{b,0}^2$ values over the territory. Statistical analyses of wind speed in several locations across the territory, or surrogate models (as in [42]) might be used to make the wind maps or the tables with $v_{b,0}$ or $v_{b,0}^2$ values.

3.4 Calibration example

A calibration example is reported in this Section for illustrating the application of the findings. The calibration was performed considering the design equation in Eq. (6) and the limit state function in Eq. (8). The probabilistic models and the PSFs are summarized in Table B1. All variables were assumed uncorrelated. Only structures loaded by permanent load and external wind pressure without dynamic effects were considered, since they represent the most common design situations.

The partial safety factor covering wind actions for the Norwegian territory was calibrated. Therefore, the uncertainties X_a affecting the $v_{b,0}^2$ values corresponding to the $v_{b,0}$ values given in the Norwegian National

Annex to EC1-1-4 were estimated. The $v_{b,0}$ values for the Norwegian territory were derived in [42] based on hindcast data collected at defined grid points over the North Sea, Norwegian Sea and Barents Sea for the period 1955-1997. In detail, sea surface pressure data were used to produce geostrophic wind data, and from the data the 10-minutes mean wind velocity averaged over area units of $75\times 75\,km^2$ was determined four times a day (at 00, 6, 12 and 18 UTC). Successively, transformation parameters calibrated against real wind records were used to transform the data to point-in-time and point-in-space values for the standard terrain roughness ($z=0.05\,m$). The Gumbel-Lieblein method was used to fit a Gumbel distribution to the generated wind speed squared data [29, 43] and deriving the $v_{b,0}^2$ values.

The uncertainty on the distribution location, X_a, is represented by a Lognormal distribution with parameters estimated with Maximum Likelihood method from the realisations $x_{a,i}$ computed according to Eq. (9), where $\left(v_{b,0}^2\right)_{M,i}$ and $\left(v_{b,0}^2\right)_{HC,i}$ are the characteristic values (98 % fractiles) obtained from in-land measured and hindcast-generated time series, respectively. The values in 21 locations on the Norwegian coast given in [42] were used for estimating the distribution parameters. The statistical uncertainty was integrated by Eq. (2), and the integral was approximated by Monte Carlo simulations. The parameters of the lognormal distribution approximating the predictive distribution were found to be $\mu_{X_a}=0.96$ and $COV_{X_a}=0.14$.

$$x_{a,i}=\frac{\left(v_{b,0}^2\right)_{M,i}}{\left(v_{b,0}^2\right)_{HC,i}} \tag{9}$$

The calibrated γ_Q was obtained solving the minimization problem in Eq. (10), where: β_i and $w_{\delta,i}$ are the reliability index and the weight associated with a certain δ_i ; $w_{m,j}$ is the weight associated with the j^{th} material, and β_t is the target reliability. A target reliability $\beta_t=4.7$ was chosen as given in [1] and in [44]. Three material properties were considered simultaneously: the structural steel yielding strength ($w_{m,1}=0.4$), the reinforced concrete compression strength ($w_{m,2}=0.4$) and the glulam timber bending strength ($w_{m,3}=0.2$). These three construction materials are the most used in Europe. The associated weights were estimated subjectively. Ten values of δ equally spaced between 0 and 1 and equally weighted represented a broad range of design situations, from light structures ($\delta=0$) to gravity-based structures ($\delta=1$). The material and permanent load PSFs were fixed, see Table B1.

$$\underset{\gamma_Q}{\operatorname{argmin}}\left\{\sum_{j=1}^{3}w_{m,j}\left[\sum_{i=1}^{10}w_{\delta,i}\left(\beta_i\left(z\left(\gamma_M,\gamma_G,\gamma_Q\right)\right)-\beta_t\right)^2\right]\right\} \tag{10}$$

The solution of the minimization problem gave γ_Q values varying from 1.57 to 1.80 in the relevant range of $COV_{V_{b,\max}^2}$ values, say $[0.15,0.5]$, see Figure 12. The selection of the $COV_{V_{b,\max}^2}$ was therefore crucial for the accurate calibration.

The limit state function in Eq. (8) with unknown $COV_{V_{b,\max}^2}$ represented by a normal distribution with $\mu_{COV_{V_{b,max}^2}}=0.25$ and $COV_{COV_{V_{b,max}^2}}=0.2$ gave $\gamma_Q\cong 1.60$. This value corresponds, with good approximation, to the PSF calibrated with known coefficient of variation equal to the mean ($COV_{V_{b,max}^2}=0.25$). In fact, the $COV_{V_{b,\max}^2}$ omission sensitivity factor [45] was found to be very close to 1, and the FORM sensitivity factor was approximatively equal to zero. Hence, the $COV_{V_{b,\max}^2}$ design point was close to its mean value. Therefore, the random variable could be substituted by its mean value in the limit state function. This made the distribution representing $COV_{V_{b,\max}^2}$ of little interest, and avoided the selection of a distribution type that is a non-trivial task since there is no theoretical evidence supporting one or another distribution. In addition, the use of the $COV_{V_{b,\max}^2}$ mean value reduced the possible values of the calibrated γ_Q to the range $[1.57,1.65]$ (corresponding to $\mu_{COV_{V_{b,max}^2}}\in[0.2,0.3]$). A conservative selection of $\mu_{COV_{V_{b,max}^2}}=0.3$ led to $\gamma_Q=1.65$ that could be considered an upper limit. The reliability indices before and after calibration are illustrated in Figure 13.

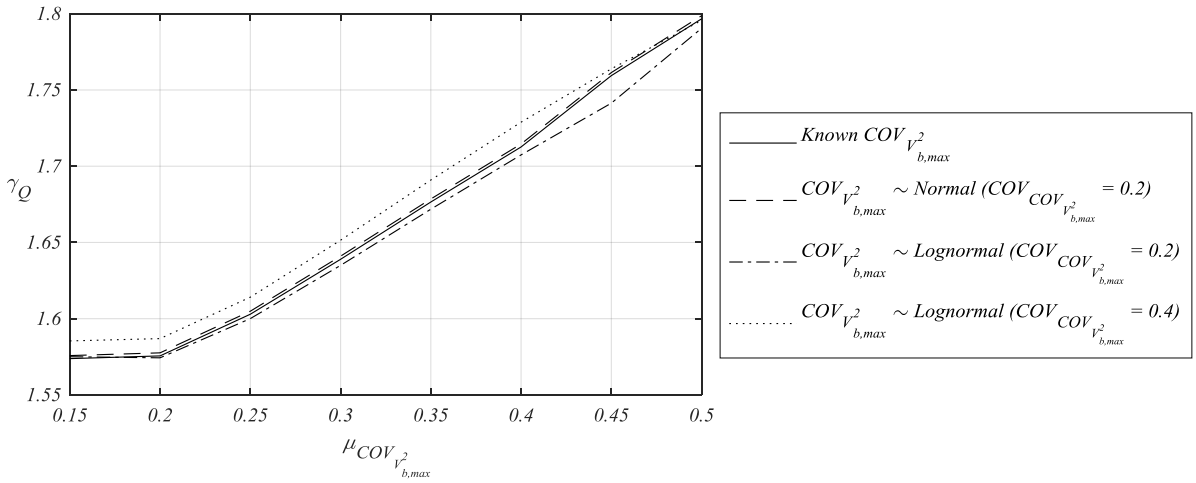

Figure 12 - Calibrated partial safety factor for wind action from the accurate calibration with Eq. (10) and the limit state function in Eq. (8).

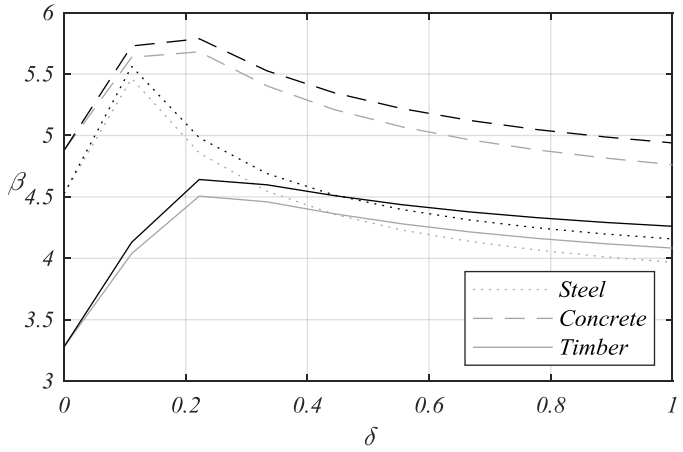

Figure 13 – Reliability indices associated with $\gamma_Q = 1.50$ *(grey lines) and* $\gamma_Q = 1.60$ *(black lines).*

4 Discussion

The accuracy and goodness of the distribution representing the wind climate were not assessed in the classical absolute sense. However, the criteria related to the accuracy and goodness were defined in Section 2.1, and a model that satisfies all these points was considered accurate, good in a Bayesian sense, i.e. as a basis for engineering decision making.

The calibration method and the probabilistic modelling approach proposed in the paper are able to account for the following epistemic uncertainties.

- The uncertainties on the choice of distribution type. These uncertainties are reduced by a careful and profound assessment of the phenomenon originating the wind and the underlying statistics. Different analyses techniques, based on various basic assumption, provide the same result.
- The uncertainties on the distribution parameters due to the limited number of measurements and the poor quality of measurements. These uncertainties are integrated into the distribution function.
- The uncertainty affecting the characteristic values of the wind maps for Norway due to their estimation with numerical model used. This uncertainty is represented by a stochastic variable that is included in the calibration of the safety factors.

The values of the partial safety factor proposed in the calculation example are sensitive to the chosen probabilistic models and are relative to the assumptions made. In particular, γ_Q is highly sensitive to both the

resistance and the wind model biases (e.g. $\mu_{X_R}, \mu_{C_{pe}} \mu_{C_g} \mu_{C_r} \mu_{C_d} \mu_{X_Q}, \mu_{X_a}$). For example, the Eurocode 1 model includes hidden safety as reported in [14]. The inclusion of the model bias is crucial for an accurate calibration. Therefore, further research and investigations are needed for modelling probabilistically the *influence of terrain*, the *aerodynamic effects* and the *dynamic effects* links of the Davenport chain in order to calibrate γ_Q more accurately. In addition, the calibration of γ_Q was performed keeping the material and self-weight partial safety factors constant. More homogeneous reliability and a different value for γ_Q would be obtained optimising all the three partial safety factors simultaneously. Nevertheless, the scope of the example was to illustrate the proposed method, rather than proposing final values of γ_Q.

5 Conclusions

The analyses of the wind data with different statistical techniques indicated the use of Gumbel distribution for representing the 10-minutes mean wind speed squared yearly maxima $V^2_{b,\max}$ in reliability analyses for calibration of design codes. All techniques indicated that this distribution is accurate in the upper tail, consistent with the underlying statistic and minimising the asymptotic errors. No theoretical evidence was found supporting the use of the three-parameters Lognormal distributions. The variations of the distribution coefficient of variation *COV* in space and for different censoring thresholds were found to be of the same order of magnitude. Values between 0.20 and 0.35 were observed for the *COV* of $V^2_{b,\max}$ in the analyses. The location or magnitude of the distribution is given in design standards through tables or wind maps. The uncertainty affecting the values provided in the Norwegian National Annex to the Eurocode 1 was estimated. A method for accounting both this uncertainty and the space-variation of the distribution coefficient of variation in the calibration of partial safety factors was proposed. The method can be used for solving similar problems in code calibration such as the space-variation of the snow load characteristics.

In a calibration exercise, it was found that the space-variation can be accounted with good approximation by using the mean value of the coefficient of variation in the reliability analyses. The use of the average parameter avoided the need of modelling the parameters variation in space probabilistically. The calibrated partial safety factor for wind actions was found to be around 1.60. The high sensitivity of the calibrated safety factor to the biases affecting the load and resistance models implemented in the codes was discussed, and the need for detailed probabilistic modelling of these uncertainties was highlighted. Although the present work focused on the European standards (Eurocodes), the analyses techniques, modelling principles and the proposed calibration method have general validity.

Appendix A. Equations and formulas

Generalised Extreme Value (GEV) distribution (support $x \in \left[a - b/\xi_{GEV}\right)$ for $\xi_{GEV} > 0$ (Fréchet); $x \in \left(-\infty, +\infty\right)$ for $\xi_{GEV} = 0$ (Gumbel) and $x \in \left(-\infty, a - b/\xi_{GEV}\right]$ for $\xi_{GEV} < 0$ (Reversed Weibull or Weibull maxima)):

$$F_X\left(x \mid \xi_{GEV}, a, b\right) = \begin{cases} \exp\left\{-\left[1+\xi_{GEV}\left(\dfrac{x-a}{b}\right)\right]^{-1/\xi_{GEV}}\right\} & \xi_{GEV} \neq 0 \\ \exp\left\{-\exp\left[-\dfrac{x-a}{b}\right]\right\} & \xi_{GEV} = 0 \end{cases} \tag{A.1}$$

Likelihood for rounded values $\hat{x}_{r,i}$ corresponding to the (unknown) measured value $\hat{x}_i \in \left(\hat{x}_i^-; \hat{x}_i^+\right]$ with: $\hat{x}_i^- = \hat{x}_{r,i} - \Delta$, $\hat{x}_i^+ = \hat{x}_{r,i} + \Delta$ and Δ being half the rounding interval.

$$L\left(\boldsymbol{\theta} \mid \hat{\mathbf{x}}_r\right) = \prod_{i=1}^{n} L\left(\boldsymbol{\theta} \mid \hat{x}_{r,i}\right) \tag{A.2}$$

With:

$$L\left(\boldsymbol{\theta} \mid \hat{x}_{r,i}\right)=\begin{cases} F\left(\hat{x}_i^{+} \mid \boldsymbol{\theta}\right)-F\left(\hat{x}_i^{-} \mid \boldsymbol{\theta}\right) & \text{if } \hat{x}_i^{-} \geq x_c \\ F\left(x_c \mid \boldsymbol{\theta}\right) & \text{if } \hat{x}_i^{+} \leq x_c \\ F\left(x_c \mid \boldsymbol{\theta}\right)\cdot \Pr\left(\hat{x}_i \in \left(\hat{x}_i^{-}; x_c\right)\right)+\left[F\left(\hat{x}_i^{+} \mid \boldsymbol{\theta}\right)-F\left(x_c \mid \boldsymbol{\theta}\right)\right]\cdot \Pr\left(\hat{x}_i \in \left(x_c; \hat{x}_i^{+}\right)\right) & \text{elsewhere} \end{cases} \tag{A.3}$$

where x_c is the censoring threshold, $\hat{\mathbf{x}}_r$ is the sample of rounded values, $\boldsymbol{\theta}$ is the vector of parameters and $\Pr(A)$ is the probability of the event A.

Weibull distribution (support $x \geq 0$):

$$F_X\left(x \mid a_w, b_w\right)=1-\exp\left[-\left(\frac{x}{a_w}\right)^{b_w}\right] \tag{A.4}$$

Generalized Pareto distribution (GPD) (support $x \geq 0$ for $\xi_{GPD} \geq 0$, $x \leq -\bar{\sigma}/\xi_{GPD}$ for $\xi_{GPD} < 0$):

$$F_X\left(x \mid \xi_{GPD}, \bar{\sigma}\right)=\begin{cases} 1-\left(1+\dfrac{\xi_{GPD} x}{\bar{\sigma}}\right)^{-1/\xi_{GPD}} & \xi_{GPD} \neq 0 \\ 1-\exp\left(-\dfrac{x}{\bar{\sigma}}\right) & \xi_{GPD} = 0 \end{cases} \tag{A.5}$$

Appendix B. Stochastic models used in the example calibration

*Table B1 – Stochastic models representing the basic random variables (from [27] unless otherwise stated) and partial safety factors ([a] [46] [b][47], [c][48], [d][49], [e][50], [f][51], [g][14], [h][1], [i][16], *range of possible values given in [27])*

	Description		**Distribution type**	**Mean**	**COV**	**Characteristic fractile**	**Partial safety factor (γ)**
X_R	Model uncertainty	Structural steel element in compression [a]	Lognormal	1.15	5 %	/	/
		Reinforced concrete element in compression [a]	Lognormal	1.20	15 %	/	/
		Glulam timber element in bending	Lognormal	1.00	15 %	/	/
R	Material property	Struct. Steel yielding strength	Lognormal	1.00	7 %	5 %	1.00 [b]
		Concrete compression strength	Lognormal	1.00	15 % [c]	5 %	1.50 [d]
		Glulam timber bending strength	Lognormal	1.00	15 %	5 %	1.25 [e]
C_r	Roughness factor		Lognormal	0.80	15 % (10 to 20%)*	$F_{C_r}\left(\mu_{C_r}\right)$	/
C_g	Gust factor		Lognormal	1.00	15 % (10 to 15%)*	$F_{C_g}\left(\mu_{C_g}\right)$	/
C_{pe}	External pressure coefficient		Gumbel [f]	1.00	25 % [g] (10-30%)*	80 % [i]	/
G	Permanent action		Normal	1.00	10 %	50 %	1.35 [h]
$V^2_{b,\max}$	Mean wind speed (1yr max)		Gumbel	1.00	$COV_{V^2_{b,max}}$	98 %	To be calibrated
X_a	$F_{V^2_{b,\max}}$ location uncertainty		Lognormal	0.96	0.14	$F_{X_a}(1)$	/
$COV_{V^2_{b,max}}$	$V^2_{b,\max}$ coefficient of variation		Normal	0.25	0.20	/	/
X_Q	Wind load model uncertainty [a]		Normal	0.80	0.20	$F_{X_Q}(1)$	/

6 References

1. European Committee for Standardization (CEN). *EN 1990:2002/A1:2005/AC:2010 Eurocode 0 - Basis of structural design*. Brussels; 2002.
2. Melchers R.E. *Structural reliability: analysis and prediction.* Second ed. Chichester, England: John Wiley & Sons Ltd.; 1999.

3. Lind N.C. *Reliability based structural codes, practical calibration*. In: Holand I., editor. *Safety of structures under dynamic loading*; Trondheim, Norway. Norwegian Institute of Technology; 1977. p. 149-60.
4. Madsen H.O., Krenk S., Lind N.C. *Methods of structural safety*. Mineaola, New York: Dover Publications; 2006. 407 p.
5. Faber M.H., Sørensen J.D. *Reliability based code calibration - The JCSS approach*. In: Der Kiureghian A., Madanat S., Pestana J.M., editors. *Proc of the 9th International Conference on Applications of Statistics and Probability in Civil Engineering*. San Francisco: Millpress; 2003. p. 927-35.
6. Vrouwenvelder T., Scholten N. Assessment criteria for existing structures. *Structural Engineering International*. 2010; **1**, pp. 4.
7. Ditlevsen O., Madsen H.O. *Structural Reliability Methods* [Monograph]: Department of Mechanical engineering at the Technical University of Denmark; 2007. Available from: http://od-website.dk//index-2.html/books.htm.
8. Davenport A.G. The relationship of reliability to wind loading. *Journal of Wind Engineering and Industrial Aerodynamics*. 1983; **13**(1–3), pp. 3-27.
9. European Committee for Standardization (CEN). *EN 1991-1-4:2005 Eurocode 1 - Actions on structures - Part 1-4: General actions - Wind actions*. Brussels; 2005.
10. Cook N.J. *The designer's guide to wind loading of building structures: static structures.* Building Research Establishment, Department of the Environment; 1990. 586 p.
11. Cook N.J. *The designer's guide to wind loading of building structures: Background, damage survey, wind data, and structural classfication.* Building Research Establishment, Department of the Environment; 1985. 371 p.
12. Botha J. *Probabilistic models of design wind loads in south africa* [Ph.D. Thesis]. Matieland, South Africa2016.
13. Holicky M., Sykora M. *Probabilistic models for wind actions*. *Proc of the Second International Symposium on Stochastic Models in Reliability Engineering, Life Science and Operations Management (SMRLO)*; 2016. p. 172-5.
14. Hansen S.O., Pedersen M.L., Sørensen J.D. *Probability based calibration of pressure coefficients*. *Proc of the 14th International Conference on Wind Engineering*. Porto Alegre, Brazil; 2015.
15. Van der Hoven I. Power spectrum of horizontal wind speed in the frequency range from 0.0007 to 900 cycles per hour. *Journal of Meteorology*. 1957; **14**(2), pp. 160-4.
16. International Organization for Standardization (ISO). *ISO 4354:2009 Wind actions on structures*. Lausanne, Switzerland; 2009.
17. Harris R.I. An improved method for the prediction of extreme values of wind effects on simple buildings and structures. *Journal of Wind Engineering and Industrial Aerodynamics*. 1982; **9**(3), pp. 343-79.
18. Der Kiureghian A. Analysis of structural reliability under parameter uncertainties. *Probabilistic Engineering Mechanics*. 2008; **23**(4), pp. 351-8.
19. Gumbel E.J. *Statistics of Extremes.* Columbia University Press; 1967.
20. Coles S. *An introduction to statistical modeling of extreme values.* London: Springer-Verlag 2004 2001. XIV, 209 p.
21. Kruger A.C., Retief J.V., Goliger A.M. Strong winds in South Africa: Part 1 Application of estimation methods. *Journal of the South African Institution of Civil Engineering*. 2013; **55**(2), pp. 29-45.
22. Norwegian Meteorological Institute (MET). *eKlima* [Available from: http://sharki.oslo.dnmi.no/portal/page?_pageid=73,39035,73_39049&_dad=portal&_schema=PORTAL].
23. Wen Y.K. Wind direction and structural reliability. *Journal of Structural Engineering*. 1983; **109**(4), pp. 1028-41.
24. Grabemann I., Weisse R. Climate change impact on extreme wave conditions in the North Sea: an ensemble study. *Ocean Dynamics*. 2008; **58**(3), pp. 199-212.
25. Madsen H.O. *Managing structural safety and reliability in adaptation to climate change*. In: Deodatis G., Ellingwood B.R., Frangopol D.M., editors. *Proc of the 11th International Conference on Structural Safety and Reliability*. London, UK: Taylor and Francis Group; 2014. p. 81-8.
26. Harris R.I. The accuracy of design values predicted from extreme value analysis. *Journal of Wind Engineering and Industrial Aerodynamics*. 2001; **89**(2), pp. 153-64.
27. Joint Committee on Structural Safety (JCSS). *Probabilistic Model Code* 2001. Available from: http://www.jcss.byg.dtu.dk/Publications.
28. Harris R.I., Cook N.J. The parent wind speed distribution: Why Weibull? *Journal of Wind Engineering and Industrial Aerodynamics*. 2014; **131**, pp. 72-87.

29. Cook N.J., Harris R.I. Exact and general FT1 penultimate distributions of extreme wind speeds drawn from tail-equivalent Weibull parents. *Structural Safety*. 2004; **26**(4), pp. 391-420.
30. Jordaan I. *Decisions Under Uncertainty: Probabilistic Analysis for Engineering Decisions.* Cambridge University Press; 2005.
31. Martins E.S., Stedinger J.R. Generalized maximum-likelihood generalized extreme-value quantile estimators for hydrologic data. *Water Resources Research*. 2000; **36**(3), pp. 737-44.
32. Akaike H. A new look at the statistical model identification. *IEEE Transactions on Automatic Control*. 1974; **19**(6), pp. 716-23.
33. Næss A., Gaidai O. Monte Carlo Methods for Estimating the Extreme Response of Dynamical Systems. *Journal of Engineering Mechanics*. 2008; **134**(8), pp. 628-36.
34. Karpa O., Naess A. Extreme value statistics of wind speed data by the ACER method. *Journal of Wind Engineering and Industrial Aerodynamics*. 2013; **112**(0), pp. 1-10.
35. Karpa O. *ACER User Guide* Online 2012 [Available from: http://folk.ntnu.no/karpa/ACER/ACER_User_guide.pdf].
36. Pickands J. Statistical inference using extreme order statistics. *The Annals of Statistics*. 1975; **3**(1), pp. 119-31.
37. Caers J., Maes M.A. Identifying tails, bounds and end-points of random variables. *Structural Safety*. 1998; **20**(1), pp. 1-23.
38. Davison A.C., Smith R.L. Models for Exceedances over High Thresholds. *Journal of the Royal Statistical Society Series B (Methodological)*. 1990; **52**(3), pp. 393-442.
39. Maes M.A. *Extrapolation into the unknown: modelling tails, extremes, and bounds*. 2003.
40. Kasperski M. Specification of the design wind load—A critical review of code concepts. *Journal of Wind Engineering and Industrial Aerodynamics*. 2009; **97**(7–8), pp. 335-57.
41. Thoft-Christensen P., Baker M.J. *Structural reliability theory and its applications.* Berlin, Heidelberg: Springer Berlin Heidelberg; 1982.
42. Harstveit K. *Extreme value analysis of hindcast wind data from the maritime areas surrounding Norway*. Norwegian Meteorological Institute; 2005, 29/11/20085. Report No.: 17/05.
43. Harris R.I. Gumbel re-visited - a new look at extreme value statistics applied to wind speeds. *Journal of Wind Engineering and Industrial Aerodynamics*. 1996; **59**(1), pp. 1-22.
44. International Organization for Standardization (ISO). *ISO 2394:2015 General principles on reliability for structures*. Switzerland; March, 2015.
45. Madsen H.O. Omission sensitivity factors. *Structural Safety*. 1988; **5**(1), pp. 35-45.
46. Holicky M., Sykora M. *Conventional probabilistic models for calibration of codes*. In: Faber M.H., Köhler J., Nishijima K., editors. *Proc of the 11th Int Conf on Applications of Statistics and Probability in civil engineering, Zurich, Switzerland, August 2011*: CRC Press; 2011. p. 969-76.
47. European Committee for Standardization (CEN). *EN 1993-1-1:2005 Eurocode 3 - Design of steel structures - Part 1-1: General rules and rules for buildings*. Brussels; 2005.
48. Sørensen J.D., Hansen S.O., Nielsen T.A. *Calibration of partial safety factors for Danish structural codes. Proc IABSE Conf Safety, Risk and Reliability–Trends in Engineering, Malta, 2001*. Zurich, Switzerland: IABSE; 2001. p. 179-84.
49. European Committee for Standardization (CEN). *EN 1992-1-1:2004 Eurocode 2: Design of concrete structures - Part 1-1: General rules and rules for buildings*. Brussels; 2004.
50. European Committee for Standardization (CEN). *EN 1995-1-1:2004/A1:2008 Eurocode 5: Design of timber structures. Part 1-1: General common rules and rules for buildings*. Brussels; 2004.
51. Cook N.J., Mayne J.R. A novel working approach to the assessment of wind loads for equivalent static design. *Journal of Wind Engineering and Industrial Aerodynamics*. 1979; **4**(2), pp. 149-64.